Ion Conduction Mechanisms and Thermal Properties of Hydrated and Anhydrous Phosphoric Acids Studied with ^{1}H, ^{2}H, and ^{31}P NMR

Yuichi Aihara,*,† Atsuo Sonai,† Mineyuki Hattori,‡ and Kikuko Hayamizu‡

Samsung Yokohama Research Institute, 2-7 Sugasawa-cho, Tsurumi-ku, Yokohama 230-0027, Japan, and National Institute of Advanced Industrial Science and Technology, AIST Tsukuba Center 5, Tsukuba, Ibaraki 305-8565, Japan

Received: July 14, 2006; In Final Form: September 28, 2006

To understand the behaviors of phosphoric acids in fuel cells, the ion conduction mechanisms of phosphoric acids in condensed states without free water and in a monomer state with water were studied by measuring the ionic conductivity (σ) using AC impedance, thermal properties, and self-diffusion coefficients (D) and spin−lattice relaxation times (T_1) with multinuclear NMR. The self-diffusion coefficient of the protons (H^+ or H_3O^+), H_2O, and H located around the phosphate were always larger than the diffusion coefficients of the phosphates and the disparity increased with increasing phosphate concentration. The diffusion coefficients of the samples containing D_2O paralleled those in the protonated samples. Since the ^{1}H NMR T_1 values exhibited a minimum with temperature, it was possible to determine the correlation times and they were found to be of nanosecond order for a distance of nanometer order for a flip. The agreement of the ionic conductivities measured directly and those calculated from the diffusion coefficients indicates that the ion conduction obeys the Nernst−Einstein equation in the condensed phosphoric acids. The proton diffusion plays a dominant role in the ion conduction, especially in the condensed phosphoric acids.

1. Introduction

The ion conduction mechanisms of phosphoric acid have been investigated widely since anomalously large ion conduction was observed in highly viscous liquid phosphoric acids. The structures of phosphoric acids are complex and related to their complicated hydrated and anhydrous forms. Fully dried H_3PO_4 (orthophosphoric acid) is a solid at room temperature with a monomer structure (H_3PO_4, P1). The addition of water does not change the monomer structure. Under anhydrous conditions, condensed structures of the dimer (pyrophosphic acid, $H_6P_2O_7$, P2), trimer (meta- or tripolyphosphoric acid, $H_8P_3O_{10}$, P3), and larger fused structures are formed. The fast ion conduction in phosphoric acids has been explained by a protonic Grotthus conduction mechanism; however, difficulties exist in explaining the gap between the fast Grotthus (hopping) and slow vehicle (diffusive) mechanisms over a wide range of H_2O content. In early works, Greenwood and Thompson interpreted the anomalous ionic conduction of the phosphoric acid by the protonic Grotthus chain mechanism.[1] Several investigations have been performed on the ion conduction in fused and dilute phosphoric acids with or without H_2O or heavy water (D_2O).[1−6] From ^{31}P and ^{1}H NMR measurements of the individual diffusion coefficients various mechanisms for the ion conduction have been proposed. Dippel et al. suggested a linkage between local and diffusive motions for H_3PO_4 by using pulsed-gradient spin−echo (PGSE) NMR and quasielastic neutron scattering (QENS).[7,8] Chang et al. reported relationships between the Stokes−Einstein and Nernst−Einstein equations for an aqueous phosphoric acid.[9] Also in a phosphoric acid doped polyethyleneoxide (i.e., a polymer protonic conductor), Donoso et al. reported relationships between long- and short-range diffusions using PGSE NMR, QENS, and NMR T_1 measurements.[10] Clearly, the ion conduction in phosphoric acid systems is carried by both phosphates (anion) and protons (H^+ and/or H_3O^+).

Nowadays, large-scale residential phosphoric acid fuel cells (PAFC) are commercially available. In the near future, compact systems are required for cogeneration and mobile applications. Polymer membranes doped with phosphoric acids have been proposed[11] for use in polymer electrolyte type fuel cell (PEFC) applications in the medium-temperature range (up to 473 K). To realize wide-scale usage of fuel cells, greater cost reduction and operation of long duration are required. In the development of the medium-temperature system, simpler water management and lower carbon monoxide poisoning of the catalysts are expected to settle such demands due to the medium operation temperature.

Condensed phosphoric acids P2 or P3 are formed from 423 to 573 K under anhydrous conditions where the liquid water is unstable and does not coexist with the condensed phosphoric acids. To design advanced PEFC and PAFC, a clear understanding of the conduction mechanisms over a wide concentration range from aqueous solutions to condensed liquids of phosphoric acid is essential, in particular the role(s) of H_2O on the ion conduction needs to be clarified.

In this paper, samples with phosphoric acid concentrations ranging from 75 to 105 wt % were prepared by adding water (H_2O) or heavy water (D_2O) to commercially available 116 wt % phosphoric acid. The 116 and 105 wt % phosphoric acid samples are anhydrous and consist of P1, P2, and P3 only. The (aqueous) 95, 85, and 75 wt % phosphate samples include P1 and H_2O. Macroscopic properties like thermogravimetry (TG), glass transition temperature (T_g) by differential scanning calorimetry (DSC), and ionic conductivity (σ) and also microscopic

* Address correspondence to this author. E-mail: yuichi.aihara@samsung.com. Phone: +81-45-510-3971. Fax:+81-45-510-3368.

† Samsung Yokohama Research Institute.

‡ National Institute of Advanced Industrial Science and Technology.

10.1021/jp064452v CCC: $33.50
Published on Web 11/18/2006

TABLE 1: The Phosphoric Acid (PA) Samples and Their Compositions

sample	H_3PO_4 (wt %)	P_2O_5 conv (wt %)	$H_2O + D_2O$[b] content (mol %)	D_2O/H_2O molar ratio	remarks
75PA	75	54	64.5		includes free
75PA-D[b]				1.87_5	water
85PA	85	61	49.0		includes free
85PA-D[b]				1.43_8	water
95PA	95	69	22.3		includes free
95PA-D[b]				0.93_8	water
105PA	105	76	0[a]		no free
105PA-D[b]				0.50_0	water
116PA	116	84	0[a]		as supplied, no free water

[a] As prepared. [b] PA-D samples were prepared by adding D_2O.

phenomena such as the individual self-diffusion coefficients (D) and spin−lattice relaxation (T_1) measured with ^1H, ^2H, and ^{31}P NMR were used to characterize the phosphoric acids. Ion conduction mechanisms over a wide concentration range from dilute aqueous solution to condensed liquids (important for practical purposes) were inferred from the experimental data.

2. Experimental Procedure

2.1. Sample Preparation. Four samples of different concentrations (75, 85, 95, and 105 wt %) of phosphoric acids (54, 61, 69, and 76 wt % in P_2O_5 conversion) were prepared by hydrolyzing 116 wt % phosphoric acid (polyphosphoric acid, 84 wt % P_2O_5, Rasa Industry, Tokyo) with super purified water or deuterium oxide (D_2O, 100.0 atom % D, Aldrich). The samples prepared with D_2O include H_2O and HOD due to proton exchange between the polyphosphoric acid and D_2O. The composition of the samples is listed in Table 1 together with the sample names. For NMR measurements, the samples were placed into 5 mm NMR microtubes (BMS-005J, Shigemi) to a height of 5 mm and flame sealed to prevent moisture adsorption. Since the various phosphoric acids, i.e., pyro, tripoly, and highly condensed phosphoric acid, are included in the concentrated samples, their concentration ratios in the sealed samples were determined by ^{31}P NMR. Polyphosphoric acids with repeat lengths greater than 3 constituted less than 1% of the samples and were ignored.

2.2. Ionic Conductivity Determination. The ionic conductivities were determined by using the AC impedance method on an Autolab PGSTAT30 (Eco Chemie) controlled by a personal computer. The phosphoric acid samples were put into a sealed glass cell with two identical platinum blocking disk electrodes. The cell constant was determined by measuring aqueous KCl standard solution. The impedance measurements were carried out from 1 Hz to 1 MHz in the temperature range from 333 to 423 K.

2.3. TG and DSC Measurements. Thermogravimetry was performed with a TG/DTA6200 thermogravimetric/differential thermal analyzer (Seiko Instruments Inc.). The samples were put into an open platinum pan and scanned from 303 to 873 K with a scanning rate of 10 deg min^{-1}. The measurements were made under Ar gas with a flow rate of 300 mL min^{-1}. DSC was performed with a DSC6200 differential scanning calorimeter (Seiko Instruments Inc.). The samples were sealed in Au plated stainless steel pans and scanned from 123 to 573 K with a scanning rate of 10 deg min^{-1}.

2.4. Specific Density. The specific densities were determined by using a 10 cm^3 pycnometer at 303, 313, 323, and 333 K. Each sample was held for 1 h at each temperature in the pycnometer before the specific volume was obtained by weighing.

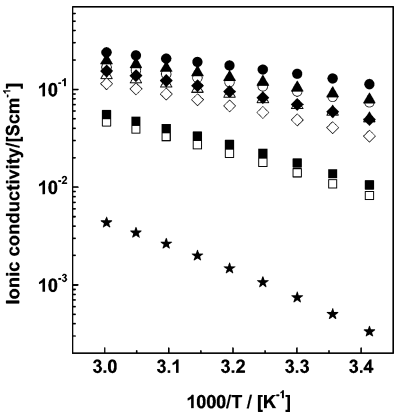

Figure 1. Arrhenius plots of the ionic conductivity for the nine samples of phosphoric acids (75PA, circle; 85PA, triangle; 95PA, diamond; 105PA, square; and 116PA, star). The solid and open symbols correspond to the PA and PA-D samples, respectively.

2.5. NMR Measurements. PGSE NMR measurements were performed on an NMR spectrometer based on a 6.35 T wide bore magnet controlled by a Tecmag Apollo system. The spectrometer was equipped with a JEOL pulsed field-gradient multinuclear probe and a JEOL current amplifier. The temperature was controlled by a JEOL console. The ^1H, ^2H, and ^{31}P measuring frequencies were 270, 41, and 109 MHz, respectively. The self-diffusion coefficients were measured by using a modified Hahn-echo sequence. The widths of the magnetic field gradient pulses were varied from 0 to 3.5 ms with the gradient amplitude ranging from 2 up to 18 T m^{-1} in order to observe a sufficient decay of the echo signals. The intervals between the leading edges of the gradient pulses (Δ) were set between 20 and 30 ms to minimize convection effects at higher temperatures. The temperature was varied between 288 and 373 K except for the 116PA sample where the temperature was changed from 303 to 403 K. For the fast diffusion of ^1H and ^2H at the higher temperatures, convection was confirmed to have negligible effects on the diffusion coefficients. As long as the PGSE attenuation profiles were purely single exponential, no significant Δ dependence was observed. An example of the ^{31}P diffusion plots is given in Figure S4 in the Supporting Information. T_1 measurements were performed by using the inversion recovery (i.e., 180°−τ−90°−Acq.) method over the wider temperature range.

3. Results

3.1. The Ionic Conductivity. Arrhenius plots of the ionic conductivity of the nine samples studied in the present paper are given in Figure 1. The ionic conductivity clearly decreased with increasing phosphoric acid concentration, especially for the 105PA and 116PA samples. The samples prepared with D_2O had lower ionic conductivities than the corresponding samples prepared with H_2O, and the difference increased in the more diluted samples (larger D_2O/H_2O ratio shown in Table 1) at higher temperatures. The temperature dependence of the ionic conductivity on the Arrhenius plots gradually changed from linear to curved as the phosphate concentration increased. The data were well-described by the Vogel−Tamman−Fulcher (VTF) equation

$$\sigma(T) = AT^{-1/2} \exp[-B/(T - T_0)] \quad (1)$$

TABLE 2: VTF Parameters and Activation Energies of the Ionic Conductivity

	VTF parameters			
sample	A [S cm^{-1} K$^{-1/2}$]	B [K]	T_0 [K]	E_a[a] [kJ mol^{-1}]
75PA	36 ± 3	305 ± 23	188 ± 5	14.6 ± 0.2
75PA-D	40 ± 5	395 ± 39	178 ± 7	16.3 ± 0.3
85PA	63 ± 10	448 ± 45	177 ± 7	18.1 ± 0.3
85PA-D	67 ± 12	527 ± 51	172 ± 7	20.0 ± 0.4
95PA	93 ± 9	546 ± 27	177 ± 3	22.3 ± 0.4
95PA-D	82 ± 9	565 ± 30	179 ± 4	24.0 ± 0.5
105PA	153 ± 11	787 ± 20	176 ± 2	32.0 ± 1.5
105PA-D	151 ± 15	806 ± 28	178 ± 2	33.4 ± 1.8
116PA	84 ± 7	1014 ± 23	187 ± 1	48.1 ± 1.1

[a] The activation energies were calculated by using the Arrhenius equation (eq 2) over the entire temperature range of measurement. The correlation coefficient (R^2) was lowest in 116 and 105 wt %, and was approximately 0.9977 in each sample.

where A and B are fitting parameters which relate to the carrier number and the configuration entropy, respectively. The third fitting parameter, T_0, is related to the glass transition temperature. The results of regressing the VTF equation onto the data are summarized in Table 2 and the correlation coefficients (R^2) were always larger than 0.9999 for all data sets. The parameters A and B increased with the phosphoric acid concentration while the T_0 values were nearly constant.

The activation energies (E_a) of the ionic conductivities in Table 2 were independently determined from the Arrhenius equation,

$$\sigma(T) = A \exp(-E_a/RT) \qquad (2)$$

where A is a constant and R is the gas constant. The E_a values increased significantly with the phosphoric acid concentration, and became three times larger in the 116PA than the 75PA samples.

3.2. DSC Measurements. Large exothermic and endothermic peaks were observed only in the 95PA sample during the heating scan (the DSC thermograms are displayed in the Supporting Information, Figure S2). The other phosphoric acids did not give any crystalline and melting peaks in the temperature range from 123 to 303 K. Since the 116PA and 105PA samples did not show any exothermic and endothermic peaks, those phosphoric acid samples might be in a supercooled state. The glass transition temperatures and the calculated values of T_0 are plotted versus the concentration in Figure 2. The glass transition temperatures could be experimentally described by a single-exponential equation, $T_g = T_g^0 + \alpha \exp(\beta c)$, where the T_g^0 is the glass transition temperature at the concentration of phosphoric acid equal to zero, the c is the concentration of the phosphoric acid, and α and β are constants. The solid line is a result of regressing the single-exponential equation on to the data (the result of the regression is discussed in the Supporting Information). The T_g of the phosphoric acids decreased linearly with the concentration, and approached T_0 of the dilute samples. The results of the thermogravimetry are shown in the Supporting Information. The relationship between the concentration and the glass transition temperature is also discussed in the Supporting Information.

3.3. ^{31}P NMR Spectra. The ^{31}P NMR spectra for 116PA, 105PA, and 85PA measured at 323 K are shown in Figure 3. The spectra of 75PA and 95PA for the P1 were almost the same as that of 85PA, except for a small peak at the P2 position in the 95PA. The ^{31}P spectra of the PA-D samples were the same as those of the PA samples. Each peak gave a single T_1 and a single self-diffusion coefficient in the temperature range measured in the present study. The P3 in the 116PA sample is composed of two terminal and one central phosphorus atom and their ^{31}P shift differences were very small. The integrated peak intensities (relative peak areas) are summarized in Table 3.

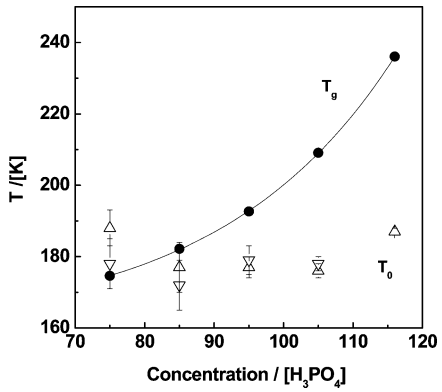

Figure 2. The glass transition temperatures measured (solid circle) for the PA samples and the calculated T_0 (up triangle: PA, down triangle: PA-D) of the phosphoric acids versus the concentration. The allowable error in T_0 was determined from the regression of the VTF equation onto the data.

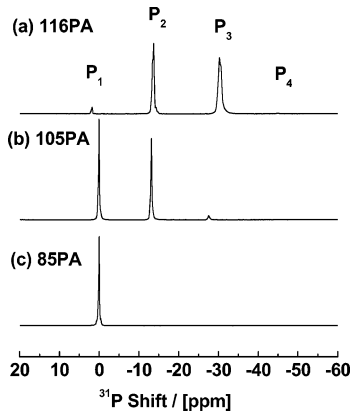

Figure 3. ^{31}P NMR spectra measured at 323 K of (a) 116PA, (b) 105PA, and (c) 85PA. A very small P4 peak was observed in the 116PA. The ^{31}P spectral patterns were insensitive to temperature.

TABLE 3: The Relative Integrated Peak Intensities of the ^{31}P NMR Spectra

samples	P1	P2	P3
75PA	100		
85PA	100		
95PA	99	1	
105PA	50	48	2
116PA	1	42	57

3.4. ^{1}H and ^{2}H NMR Spectra. The ^{1}H and ^{2}H signals were all broad single lines in the temperature range studied and the chemical shifts are summarized in Table S1 in the Supporting Information. Fast exchange, on the NMR time scale, occurs between the phosphate OH and the bulk H_2O or D_2O. The large low-field shift of 7.73 ppm referred to external H_2O for the 116PA moved to higher field as the concentration decreased. The ^{2}H shifts exhibited similar trends to the ^{1}H shifts with phosphate concentration. The ^{1}H isotope shifts induced with the D_2O addition became a little larger as the relative concentration of D_2O increased in the aqueous solution samples.

3.5. Self-Diffusion Coefficients of the Individual Components. The temperature dependencies of the self-diffusion coefficients of the 95PA and 95PA-D samples measured with

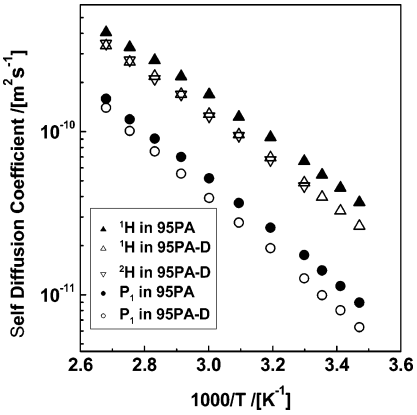

Figure 4. The self-diffusion coefficients of the individual components of the 95 wt % samples: ^{31}P (circle) and ^{1}H (up-triangle) and ^{2}H (down-triangle); the solid and open symbols correspond to PA and PA-D, respectively. D_2O diffusion could not be measured at the lower temperatures because of the short ^{2}H T_1.

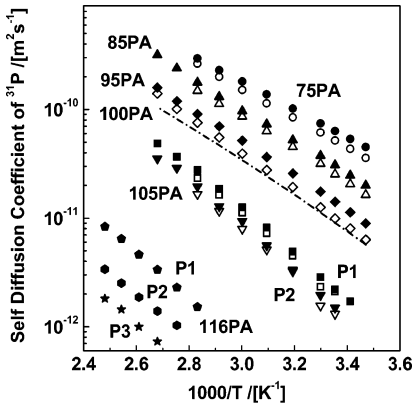

Figure 5. The temperature dependencies of the self-diffusion coefficients of the phosphates: P1 of 75PA (circle), 85PA (up triangle), 95PA (diamond), 105PA (square), and 116PA (pentagon); P2 of 105PA (down triangle) and 116PA (hexagon); and P3 of 116PA (star). The solid symbols indicate ^{31}P diffusion in PA samples and the open symbols indicate ^{31}P diffusion in the PA-D samples. The dotted line for the 100PA was calculated from literature values.[7]

^{1}H, ^{2}H, and ^{31}P NMR are shown in Figure 4. The ^{1}H diffusion coefficient (in both the PA and PA-D samples) is always larger than the phosphate diffusion coefficient and the ratios of D_H/D_{P1} were about 2.5 and 3.8 at 373 and 303 K, respectively. Generally the diffusion coefficients of the water and the phosphates in the PA samples were a little larger than those in the PA-D samples, due to the larger viscosity in the heavy water samples.[5] At each concentration of the PA-D samples, the self-diffusion coefficients measured with ^{1}H and ^{2}H NMR agreed well, especially at higher temperatures. In each PA sample, the ^{1}H diffusion coefficients were always faster than the ^{31}P diffusion coefficients in the temperature range measured.

The change in self-diffusion coefficients with temperature of the phosphates of the nine samples is shown in Figure 5, together with the literature values for 100PA.[7] With increasing water content the phosphate diffusion becomes faster and the difference between the PA and PA-D samples decreases. The 75PA, 85PA, and 95PA samples showed a single ^{31}P NMR signal for P1 and their echo attenuations were single exponential in the temperature range from 288 to 373 K, while the ^{31}P echo attenuation profiles of the P1 and P2 of the 105PA (or 105PA-D) were nonexponential below 278 K for the shorter Δ time. Also the P1, P2, and P3 echo attenuation profiles of the 116PA were nonexponential at the lower temperatures, indicating that the phosphorus diffusion is restricted. The ^{31}P self-diffusion coefficients in Figure 5 were measured in the higher temperature range where the echo attenuation profiles were single exponential. In the 116PA and 105PA (also 105PA-D) samples, different diffusion coefficients were measured for each peak and the diffusion coefficient was in the order P1 > P2 > P3 according to their molecular weights. The Arrhenius plots of the phosphate diffusion are almost linear and the activation energies calculated from Figure 5 are given in Table 4.

TABLE 4: The Activation Energies for the Diffusion Coefficients of ^{31}P, ^{1}H, and ^{2}H NMR (kJ mol^{-1})

samples	P1	P2	P3	^{1}H	^{2}H
75PA	24.5 ± 0.1			21.7 ± 0.2	
75PA-D	25.6 ± 0.1			23.3 ± 0.1	22.9 ± 0.3
85PA	28.5 ± 0.3			24.3 ± 0.3	
85PA-D	28.5 ± 0.3			25.6 ± 0.4	25.8 ± 0.5
95PA	29.8 ± 0.2			25.3 ± 0.3	
96PA-D	32.2 ± 0.1			26.8 ± 0.3	26.7 ± 0.1
105PA	38.8 ± 0.6	39.8 ± 0.8		32.4 ± 0.5	
105PA-D	39.6 ± 1.1	41.3 ± 1.3		36.0 ± 0.6	*c*
116PA	40.6 ± 0.7	36.1 ± 0.6	38.6 ± 2.0	36.1 ± 0.6[a]	
				46.3 ± 0.9[b]	

[a] Above 303 K. [b] Below 303 K. [c] The ^{2}H diffusion coefficients were not observed due to the short T_1 values.

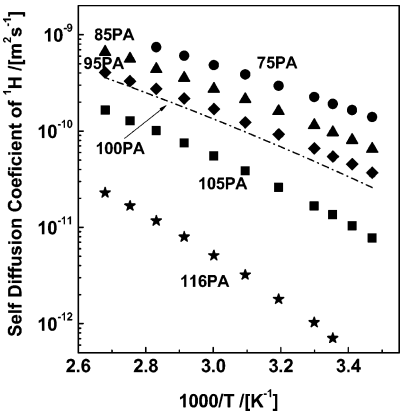

Figure 6. The temperature dependence of the ^{1}H diffusion for 75PA (circle), 85PA (triangle), 95PA (diamond), 105PA (square), and 116PA (star). The dotted line was calculated by using the proton diffusion coefficients of 100PA reported by Dippel and co-workers.[7]

The temperature dependencies of the self-diffusion coefficients measured by ^{1}H NMR of all the samples are shown in Figure 6 (the self-diffusion coefficients of ^{1}H and ^{2}H in PA-D samples are given in the Supporting Information, Figure S5), and the literature values of 100PA are also included. The hydrogen diffusion is a little faster in the PA samples than the corresponding PA-D samples probably due the larger viscosity of D_2O.[5] The fact that the self-diffusion coefficients of the hydrogen and deuterium in the PA-D samples were almost the same suggests homogeneous mixing of D_2O, HOD, and H_2O. The temperature dependencies of the hydrogen diffusion of each of the samples resemble those of the ionic conductivity (Figure 1), although a greater temperature range was possible for the diffusion measurements because of the use of sealed NMR samples. The Arrhenius plots of the hydrogen (and deuterium) diffusion coefficients are almost linear. The activation energies calculated from Figure 6 (and Figure S5) are summarized in Table 4. A larger E_a value was obtained in the lower temperature range for the 116PA sample, probably due to the restricted phosphate diffusion.

The activation energies of the P1 and the hydrogen diffusion increases with concentration and the differences between the

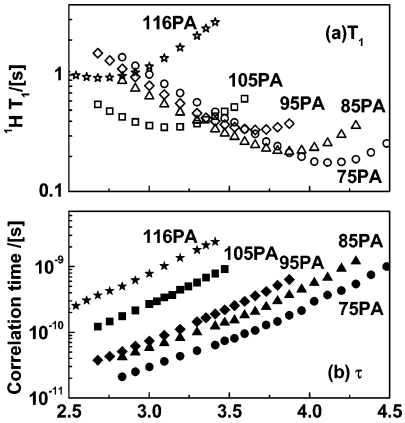

Figure 7. The temperature dependence of (a) the ^{1}H T_1 and (b) the correlation time calculated from the BPP equation (eq S1, Supporting Information) for the PA samples.

PA and PA-D samples were small. Within the same samples, the phosphate diffusions had larger activation energies than the hydrogen diffusion. The activation energies of the hydrogen diffusion in the PA samples were typically a little smaller than that of the PA-D samples, where the activation energy of hydrogen and deuterium diffusion coefficients in the PA-D samples were similar.

3.6. T_1 of ^{1}H, ^{2}H, and ^{31}P NMR. The ^{1}H NMR spin−lattice relaxation (T_1) profiles were single exponential and the temperature dependencies are shown for the PA samples in Figure 7a and for the PA-D samples in Figure S6a in the Supporting Information. Surprisingly, a T_1 minimum was observed in the liquid samples. The 116PA sample exhibited a T_1 minimum at 373 K and the minimum moved to lower temperatures with decreasing phosphate concentration. The most dilute 75PA has a T_1 minimum at 243 K. The ^{1}H T_1 values for the PA-D samples (see Figure S6a) were always longer than the corresponding PA at the same temperature. Since the gyromagnetic ratio of ^{2}H NMR is about 1/6.5 of that of the ^{1}H NMR, the longer T_1 values in the PA-D samples suggest that the ^{1}H−^{1}H or ^{1}H−^{2}H dipole−dipole interactions are the dominant relaxation mechanisms. The T_1 values and the temperatures at the minimum points are summarized for the all samples in Table S2 in the Supporting Information.

When the minimum T_1 is observed the Bloembergen Purcell Pound (BPP) equation[12] can be applied to obtain the correlation time, τ_c (the details are given in the Supporting Information). The calculated τ_c values obtained from the T_1 values are shown in Figure 7b. Although the τ_c values of the 105PA and 105PA-D samples were almost the same, the τ_c of the PA became shorter than the corresponding PA-D sample and the trend enhanced as the ratio of the D_2O contents increased in the dilute samples. The activation energies of the correlation time of the ^{1}H NMR are summarized in Table 5. Although the Arrhenius plots of the τ_c of the condensed samples were linear, those of the 85PA and 75PA samples were curved, and gave a little larger activation energy at lower temperatures as shown in Table 5.

The T_1 values of ^{31}P NMR were between 0.5 and 4 s and their temperature dependencies were very complex, which indicates the ^{31}P relaxation mechanisms include ^{31}P−^{1}H, ^{31}P−^{2}H, and ^{31}P−^{31}P interactions which greatly complicates precise determination of the molecular motions of the phosphates.

4. Discussion

4.1. Hydrolysis and the Status of the Water in the Phosphoric Acids. It is known that the 100PA (H_3PO_4, 100 wt % phosphoric acid) is a strongly hygroscopic solid (melting point 315 K) and exhibits supercooling.[7] In this study the condensed phosphoric acid 116 wt % (116PA, supercooled liquid at room temperature) was used as the starting material and with the hydrolysis decomposition, and all samples were prepared by adding water or heavy water. The phosphoric acids 116 wt % (116PA) and 105 wt % (105PA) contain inclusions of dimer (P2), trimer (P3), tetramer, or larger phosphates. No water is presumed to exist in those samples. The existence of free water can be assumed in samples less than 95 wt % (95PA). Since the thermogravimetry traces in Figure S1 show no weight loss until 373 K in the 116PA and 105PA samples, an anhydride is formed around 423 K, and gradually changes to P2 by 473 K, and then P3 is formed above 573 K. On the other hand, the weight loss observed below 373 K for the aqueous samples (95PA to 75PA) was due to the free water. Since no critical change in the TG traces (Figure S1, Supporting Information) were observed in any of the samples, a smooth hydrolysis can be presumed for those samples and the proton exchange between various phosphoric acids can easily occur, as supported by a single peak in the ^{1}H NMR spectrum.

TABLE 5: The Activation Energies (kJ mol^{-1}) for the Correlation Times (τ_c) Determined from the ^{1}H and ^{2}H NMR T_1 Measurements

samples	^{1}H NMR (τ_c) [kJ mol^{-1}] higher temp	^{1}H NMR (τ_c) [kJ mol^{-1}] lower temp	^{2}H NMR (T_1) [kJ mol^{-1}]
116PA	21.5 ± 0.2		
105PA	21.2 ± 0.2		-
105PA-D	21.8 ± 0.4		33.5 ± 0.9
95PA	19.6 ± 0.2		
95PA-D	19.5 ± 0.3		27.1 ± 0.5
85PA	15.7 ± 0.1	23.4 ± 0.4[a]	-
85PA-D	15.8 ± 0.1	21.2 ± 0.6[b]	25.8 ± 0.4
75PA	16.1 ± 0.1	22.8 ± 0.5[a]	
75PA-D	13.5 ± 0.1	20.5 ± 0.7[b]	23.0 ± 0.4

[a] Below 273 K. [b] Above 283 K.

4.2. Ion Conduction Mechanisms and Free Volume Theory. The results of regressing the VTF equation onto the ionic conductivity data in this study confirmed the relationship between the macroscopic viscosity of the phosphoric acids and total ionic conductivities. The fitting parameter T_0 is believed to be related to the glass transition temperature T_g and due to the convergence of the distributed thermal motion usually T_0 appears experimentally at a lower temperature than T_g. In this study as shown in Figure 2, T_g was mostly higher than T_0 for 85PA to 116PA and increased significantly with concentration, and at lower concentration T_g approached T_0. Generally, fast motions in the low temperatures affect T_0. The ionic conduction in the 116PA and 105PA samples must be reflected by the faster proton motions rather than the macroscopic molecular motions related to T_g. The parameter B in Table 2 that relates to the activation energy of the reorientation in the configuration of the phosphoric acids continuously changed with the concentration. The ionic conductivity is induced by the faster modes of the thermal motion and strongly depends on the configuration entropy in both fused phosphoric acids and aqueous solutions. In other words, the ionic conductivity strongly depends on the viscosity, although the anomalous fast ion conductivity is observed in all of the samples. Additionally, the parameter A closely follows the carrier number and increases with the concentration (see Figure S7, Supporting Information).

4.3. Nernst−Einstein Relationship: A Relationship between σ and D. Previously, the Walden product[2] and Stokes−Einstein[9] and Nernst−Einstein relations[7] have been applied in

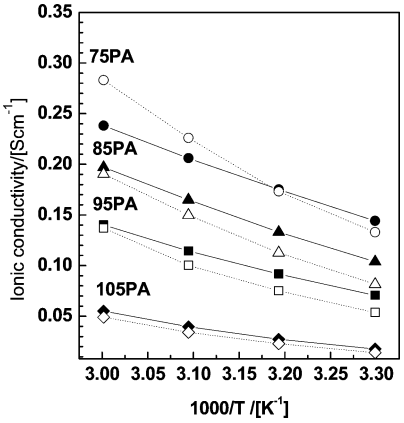

Figure 8. Arrhenius plots of the calculated ionic conductivity (σ_{N-E}, open symbols) and experimentally measured ionic conductivity (σ_{obs}, solid symbols) for 75PA (circle), 85PA (triangle), 95PA (square), and 105PA (diamond). The solid and dotted lines are guides for the eyes. The plots of the deuterium samples and 116PA are given in Figure S6 and S7, respectively.

attempting to clarify the ion conduction mechanism in aqueous and fused phosphoric acid. In this study, we assume that the ions [H^+] and [$H_2PO_4^-$] (P1) are charge carriers in calculating the conduction for the concentration range from 75 to 95 wt %. Since the P1, P2, or P3 coexist in the 105PA and 116PA samples, 2[H^+] and 3[H^+] were assumed for P2 ($H_4P_2O_7 \rightarrow 2H^+ + H_2P_2O_7^{2-}$) and P3 ($H_5P_3O_{10} \rightarrow 3H^+ + H_2P_3O_{10}^{3-}$), respectively (1:1, 2:1, and 3:1 electrolytes were assumed for the P1, P2, and P3, respectively). The ratio of the P1, P2, and P3 determined by NMR in Table 3 was used for the 105PA and 116PA. In the present case, the Nernst−Einstein equation is given by

$$\sigma_{N-E} = \frac{e^2}{kT}[\xi N_{H^+} D_{H^+} + N_{anion}(|z_{P1}|n_{P1}D_{P1} + |z_{P2}|n_{P2}D_{P2} + |z_{P3}|n_{P3}D_{P3})] \quad (4)$$

where k is the Boltzmann constant, e is the electron charge, N_{H^+} is the number of protons, N_{anion} is the number of anions, which is determined from an average molecular weight of phosphoric acids, and n_{P_x} is the relative ratio of phosphates, which was calculated from the integration ratio (Table 3) and the number of phosphorus atoms in the anions. Hence, the ratios of n_{P1}, n_{P2}, and n_{P3} are 0.67, 0.32, 0.01 and 0.02, 0.51, 0.46 for 105PA and 116PA, respectively. z_{P1}, z_{P2}, and z_{P3} are the charge number of the anions (= −1, −2, −3), and ξ corresponds to the average release number of proton from the anions and is equal to $|z_{P1}|n_{P1} + |z_{P2}|n_{P2} + |z_{P3}|n_{P3}$, where D_{H^+}, D_{P1}, D_{P2}, and D_{P3} are the self-diffusion coefficients of H^+, P1, P2, and P3, respectively. They are 1.34 and 2.42 for 105PA and 116PA, respectively (some additional data and further explanation are given in the Supporting Information).

Assuming that the diffusion coefficients measured by ^{1}H NMR correspond to the proton (H^+) diffusion (in other words, the diffusion coefficients of the neutral hydrogen atoms are assumed to be the same as the charged one), the ion conduction can be calculated by using eq 4. The results are plotted together with the measured ionic conductivity in Figure 8 in the temperature range from 303 to 333 K for 75PA, 85PA, 95PA, and 105PA. The calculated values for the PA-D samples over the same temperature range and 116PA over a higher temperature range are given in Figure S8 and Figure S9, respectively, in the Supporting Information.

At 333 K, the calculated (σ_{N-E}) and measured (σ_{obs}) ion conductivities agreed within experimental error for the 105PA, 105PA-D, 95PA, 95PA, and 85PA samples. When the temperature decreased to 303 K, the agreements were kept for the 105PA and 105PA-D. At the higher temperatures, the values of σ_{N-E} and σ_{obs} of the 116PA agreed very well. The good agreements in the condensed phosphoric acids indicate that all the phosphates behave as anions and the counter protons contribute to ionic conductivity. We have reported the agreement of σ_{N-E} and σ_{obs} for lithium salts dissolved in nonaqueous solutions by extrapolation to infinite dilution, where the ions are fully dissociated.[13] The phosphoric acids apparently diffuse as dissociated acids like isolated anions and protons. In an equilibrium state, the dissociation of phosphoric acids is known to be very small in condensed acids, e.g., the first dissociation constant of the phosphoric acid (P1) is about 7.50×10^{-3} M (at 298 K).[14] However, the concept of "dissociation in equilibrium states" does not make sense for ion conduction. It has been suggested that the phosphoric acid in an equilibrium state has a distorted tetrahedron structure with three longer P—O bonds and one shorter P═O bond.[15−18] On the other hand, a symmetrical tetrahedron structure in pure liquid phosphoric acid has been suggested from neutron diffraction.[18] A regular tetrahedron structure for concentrated aqueous solution was determined from Raman scattering, X-ray diffraction, and neutron diffraction data.[19] These data indicate the delocalization of H^+ with four equivalent oxygen atoms for the phosphate. A proton (H^+) on a phosphoric acid is delocalized near the phosphate anion in a different form from the so-called "association of acid" in the fused and the concentrated phosphoric acids. The conduction process is based on proton exchange like fast Grotthus conduction through the proton network, with the mechanism being completely vehicle (bare proton diffusion) conduction explained by the Nernst−Einstein theory.

In the aqueous phosphoric acids, the differences between the calculated and the measured ionic conductivities became a little larger in the 95PA and 85PA samples at lower temperatures where the measured values are larger. The 75PA showed a larger calculated ionic conductivity at higher temperatures. In aqueous solutions, the H_2O signal measured with ^{1}H NMR includes various diffusive species like H_2O, H^+, and H_3O^+, since it is well-known that the water including anion acts as a base and produces oxonium ions.[8] In this situation, a two-ion conduction mechanism is assumed: the protons (H^+ or H_3O^+) diffuse slower than the abundant neutral H_2O. The averaged diffusion coefficients are enhanced by the free water diffusion, although it does not guarantee fast exchange between H_2O and H^+ or H_3O^+. The conduction mechanism gradually changes with increasing H_2O population where the H^+ or H_3O^+ may diffuse in clusters in aqueous solutions. It should be noted that the differences between the experimental and calculated ionic conductivities in the $\sigma_{obs}/\sigma_{N-E}$ were larger in the PA-D samples in the D_2O-rich region (see the Supporting Information, Figure S8 and Table S3).

4.4. Diffusion Species in Condensed and Aqueous Phosphoric Acids. It is well-known that H_3O^+ is the dominant species in proton conduction when there is a large amount of free water in the aqueous phosphoric acids, whereas in fused phosphoric acids, the dominant ion conduction species is H^+. The Stokes−Einstein equation can be used to estimate the ratio of the hydrodynamic radius (r_P/r_H) for phosphate r_P and hydrogen r_H, from the ratio of D_H/D_P. The calculated ratio of D_H/D_{P1} at 313 K is plotted against concentration in Figure 9. The ratio of 100PA measured by Dipple and Kreuer[7] fits our

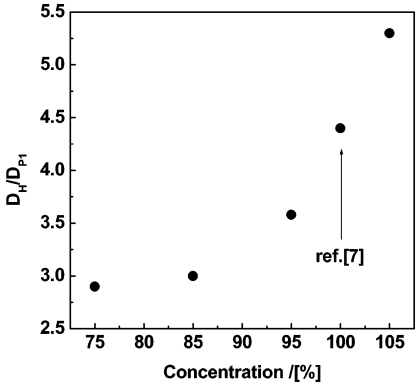

Figure 9. The ratio D_H/D_{P1} at 313 K versus the concentration of phosphoric acid. The datum for 100PA is the literature value.[7]

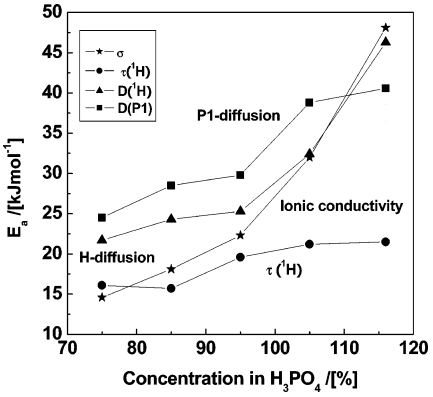

Figure 10. Activation energies of the ionic conductivity $E_a(\sigma)$, the correlation time $E_a(\tau_c)$, and the self-diffusion coefficient of the components $E_a(D)$ versus concentration for the PA samples.

data. (The experimental D_H/D_{P1} values are temperature dependent as shown in Figure S10 in the Supporting Information). Assuming that the hydrodynamic radius is proportional to the cube root of the molecular weight, $\sqrt[3]{MW}$, the relative radii assumed from the molecular weights for P1, H_3O^+, and H^+ are 4.61, 2.67, and 1, respectively. The calculated values are $r_{P1}/r_{H_3O} = 1.7$ and $r_{P1}/r_H = 4.6$. The smaller D_H/D_P values correspond to larger H_3O^+ contributions. The diffusion mechanism from the fused phosphates to aqueous phosphoric acids gradually changed from the dominant bare proton (H^+) to oxonium ion (H_3O^+) (or charged water cluster) with the increase of H_2O.

Although the diffusion coefficients of the hydrogen and the P1 are much reduced in the 105PA and 116PA samples, the relative hydrogen diffusion becomes faster in the fused phosphoric acids, and this trend was enhanced as the temperature decreased. The reduction of the diffusion of P1, P2, and P3 is probably due to the larger viscosity, while the H^+ diffusion is less influenced by the bulk viscosity. Actually the ^{31}P PGSE NMR measurements showed greatly reduced phosphate diffusion at lower temperatures.

4.5. The Effect of H_2O on Ionic Conductivity. The activation energies of the ionic conductivity $E_a(\sigma)$, self-diffusion coefficients of P1 $E_a(D_P)$ and the hydrogen $E_a(D_H)$, and the ^1H correlation time $E_a(\tau_c)$ are plotted in Figure 10. All the values increased as the concentration of the phosphates increased, with $E_a(\sigma)$ being the most sensitive to the phosphate concentration. A similar trend was observed in the PA-D samples (see Supporting Information, Figure S12). The H_2O contents clearly affect the thermal activation process of the ionic conductivity. The correlation times obtained from the ^1H T_1 varied from 10^{-11} to 10^{-9} s depending on the temperature and the phosphate concentration and each motion corresponds to a one-flip process measured with QENS.[19] It is remarkable that for 75PA $E_a(\sigma)$ is a little smaller than $E_a(\tau_c)$. That $E_a(\sigma)$ and $E_a(\tau_c)$ are similar in the dilute samples (75PA and 85PA) suggests that the ion conduction is influenced significantly by the one-flip process through water molecules such as H_2O to H_3O^+ and H_3O^+ to H_2O, which is easily thermally activated compared with the bodily hydrogen diffusion. The successive one-flip processes contribute significantly to the ionic conduction, which is related to the Grotthus mechanism. Increasing H_2O concentration decreases the viscosity and at the same time decreases the total carrier density. The large amount of water included in 75PA randomizes the hydrogen bond structure and thus enhances the thermal activation.

As the H_2O content decreases, the thermal activation energy of the one-flip process was almost unchanged and remained small in the fused phosphate, although the correlation time became longer with the phosphate concentration as shown in Figure 7. As the concentration increased, the $E_a(\sigma)$ increased significantly, and approached $E_a(D_H)$ in 105PA and 116PA. Although for 116PA the phosphorus diffusion is much slower than the proton diffusion, $E_a(D_P)$ is smaller than $E_a(D_H)$ probably due to different thermal processes controlling the proton and phosphorus diffusion. Hence, the proton diffusion determines the ion conduction in the fused phosphate systems, which is consistent with the good agreement of σ_{N-E} with σ_{AC} (Figure 8).

5. Conclusion

All of the parameters obtained from the ionic conductivity, ^1H and ^{31}P NMR diffusion, and ^1H relaxation time measurements vary smoothly with phosphoric acid concentration from 116 to 75 wt %, and the literature values of the parameters for the 100 wt % phosphoric acid fit well with the present results. In the condensed samples without free water, the ion conduction is induced by proton bodily diffusion, where the phosphate diffusion is relatively very slow. The ion conduction and the ion diffusion can be connected by the Nernst−Einstein equation (which corresponds to the vehicle mechanism) with good precision. In the aqueous phosphoric acids, H_3O^+ is one of the proton carriers and additionally relatively fast phosphate (anion) diffusion contributes to the ionic conductivity. The fast local motions of proton one-flip processes through water molecules determine the ionic conductivity, which processes are related to the so-called Grotthus mechanism. However, not all of the ions contribute to the ionic conductivity due to clustering with the water.

Acknowledgment. The authors express their sincere thanks to Professor W. S. Price for reading the manuscript critically and fruitful discussion.

Supporting Information Available: Data for the samples including heavy water, the Nernst−Einstein calculations, NMR data, and also TG and DSC traces. This material is available free of charge via the Internet at http://pubs.acs.org.

References and Notes

(1) Greenwood, N. N.; Thompson, A. *J. Chem. Soc.* **1959**, 3485.
(2) Chin, D.-T.; Chang, H. H. *J. Appl. Electrochem.* **1989**, *19*, 95.
(3) Wydeven, T. *J. Chem. Eng. Data* **1966**, *11*, 174.
(4) MacDonald, D. I.; Boyack, J. R. *J. Chem. Eng. Data* **1969**, *14*, 380.

(5) Chakrabarti, H. *J. Phys.*: *Condens. Matter* **1996**, *8*, 7019.
(6) Tsurko, E. N.; Neuland, R.; Barthel, J.; Apelblat, A. *J. Solution Chem.* **1999**, *28*, 973.
(7) Dippel, T.; Kreuer, K. D.; Lassegues, J. C.; Rodriguez, D. *Solid State Ionics* **1993**, *61*, 41.
(8) Dippel, T.; Kreuer, K. D. *Solid State Ionics* **1991**, *46*, 3.
(9) Chung, S. H.; Bajue, S.; Greenbaum, S. G. *J. Chem. Phys.* **2000**, *112*, 8515.
(10) Donoso, P.; Gorecki, W.; Berthier, C.; Defendini, F.; Poinsignon, C.; Armand, M. B. *Solid State Ionics* **1988,** *28*−*30*, 969.
(11) Wainright, J. S.; Wang, J. T.; Savinell, R. F.; Litt, M. H. *J. Electrochem. Soc.* **1995**, *142*, L121.
(12) (a) Traficante, D. D. In *An Introduction*: *Encyclopedia of Nuclear Magnetic Resonance*; Grant, D. M., Harris, R. R., editors-in-chief; John Wiley and Sons, New York, **1996**; Vol. 6, p 3988. (b) Bloembergen, N; Purcell, E. M.; Pound, R. V. *Phys. Rev.* **1948**, *73*, 679.
(13) Aihara, Y.; Sugimoto, K.; Price, W. S.; Hayamizu, K. *J. Chem. Phys.* **2000**, *113*, 1981.
(14) Greenwood, N. N.; Earnshaw, A. *Chemistry of the Elements*: Pergamon: New York, 1984.
(15) Furberg, S. *Acta Chem. Scand.* **1955**, *9*, 1557.
(16) Blessing, R. H. *Acta Crystallogr. B* **1988**, *44*, 344.
(17) Mighell, A. D.; Smith, J. P.; Brown, W. E. *Acta Crystallogr. B* **1969**, *25*, 776.
(18) Tromp, R. H.; Spieser, S. H.; Neilson, G. W. *J. Chem. Phys.* **1999**, *110*, 2145.
(19) Kameda, Y.; Sugawara, K.; Hosaka, T.; Usuki, T.; Uemura, O. *Bull. Chem. Soc. Jpn.* **2000**, *73*, 1105.
(20) Lassègues, J. C.; Cavagnat, D. *Physica* **1992**, *B180*/*181*, 645.
(21) Couchman, P. R. *Polym. Eng. Sci.* **1984**, *24*, 135
(22) Velikov, V.; Borick, S.; Angell, C. A. *Science* **2001**, *294*, 2335
(23) Stejskal, E. O.; Tanner, J. E. *J. Chem. Phys.* **1965**, *42*, 288.